



1 **Influence of Warming and Atmospheric Circulation Changes on**
2 **Multidecadal European Flood Variability**

3

4 Stefan Brönnimann,^{1,2,*} Peter Stucki,^{1,2} Jörg Franke,^{1,2} Veronika Valler,^{1,2} Yuri Brugnara,^{1,2} Ralf
5 Hand,^{1,2} Laura C. Slivinski,^{3,4} Gilbert P. Compo,^{3,4} Prashant D. Sardeshmukh,^{3,4} Michel Lang,⁵ Bettina
6 Schaeffli^{1,2}

7

8 ¹ Oeschger Centre for Climate Change Research, University of Bern, Switzerland

9 ² Institute of Geography, University of Bern, Switzerland

10 ³ University of Colorado, CIRES, Boulder, USA

11 ⁴ NOAA Physical Sciences Laboratory, Boulder, USA

12 ⁵ INRAE, Lyon-Villeurbanne, France

13 * corresponding author: stefan.broennimann@giub.unibe.ch

14

15 **Abstract**

16 European flood frequency and intensity change on a multidecadal scale. Floods were more frequent in
17 the 19th (Central Europe) and early 20th century (Western Europe) than during the mid-20th century and
18 again more frequent since the 1970s. The causes of this variability are not well understood and the
19 relation to climate change is unclear. Palaeoclimate studies from the northern Alps suggest that past
20 flood-rich periods coincided with cold periods. In contrast, some studies suggest that more floods
21 might occur in a future, warming world. Here we reconcile the apparent contradiction by addressing
22 and quantifying the contribution of atmospheric processes to multidecadal flood variability. For this,
23 we use long series of annual peak streamflow, daily weather data, reanalyses, and reconstructions. We
24 show that both changes in atmospheric circulation and moisture content affected multidecadal changes
25 of annual peak streamflow in Central and Western Europe over the past two centuries. We find that
26 during the 19th and early 20th century, atmospheric circulation changes led to high peak values of
27 moisture flux convergence. The circulation was more conducive to strong and long-lasting
28 precipitation events than in the mid-20th century. These changes are also partly reflected in the
29 seasonal mean circulation and reproduced in atmospheric model simulations, pointing to a possible
30 role of oceanic variability. For the period after 1980, increasing moisture content in a warming
31 atmosphere led to extremely high moisture flux convergence. Thus, the main atmospheric driver of
32 flood variability changed from atmospheric circulation variability to water vapour increase.

33



34 **1. Introduction**

35 Changes in flood frequency and intensity depend on many factors (Hall, 2014; Tarasova, 2019)
36 including changes in atmospheric processes such as moisture flux, convection, precipitation at
37 different time scales, changes in hydrological processes such as infiltration or overland flow, the
38 seasonal coincidence of snow melt and heavy precipitation, and on human interventions such as river
39 bed and lake regulations, hydropower plants or other hydraulic constructions. Some of these factors
40 are affected by climate change, but also multidecadal variations of climate play a role. During the 19th
41 century, floods were more frequent in Alpine countries (Glaser et al., 2004, 2010; Brázdil et al., 2005;
42 Blöschl et al., 2020, Schmocker-Fackel and Naef, 2010a,b; Himmelsbach et al., 2015; Lang et al.,
43 2016) triggering political discussion that led to legislation on forest conservation and hydraulic
44 engineering (Summermatter, 2005). In contrast, floods were comparably rare in Central Europe in the
45 mid-20th century, a period when large infrastructure projects were planned and carried out (Pfister
46 2009). The causes of this multidecadal flood variability are not well understood. Atmospheric
47 circulation changes played a role (Jacobeit et al., 2003; Mudelsee et al., 2004; Quinn and Wilby, 2013;
48 Brönnimann et al., 2019), but this has not been well quantified. Furthermore, the relation to climate
49 change is unclear. In this paper we analyse multidecadal flood variability in Europe in relation to
50 atmospheric processes and in particular their link to climate change.

51 Better understanding this relation is relevant for assessing future flood risk. For this it is important to
52 settle a long-standing controversy: While palaeoclimate studies (Stewart et al., 2011; Glur et al., 2013;
53 Engeland et al., 2020) from the northern Alps or Norway suggest that past flood-rich periods
54 coincided with cool periods, climate projections suggest that with global warming, flood occurrence
55 will increase globally and in the majority of regions (Alfieri et al., 2017). Our paper addresses this
56 question by applying a dynamical perspective to a long period (200 years) that covers both types of
57 flood periods.

58 In this paper we specifically focus on the atmospheric contribution to flood variability. In particular,
59 we explore to what extent atmospheric processes can explain multidecadal variability in flood
60 intensity. We also investigate how the atmospheric contribution can be further partitioned into
61 contributions from circulation changes and moisture changes. To achieve this, we analyze long annual
62 peak streamflow series, daily weather data, reanalyses, and reconstructions.

63

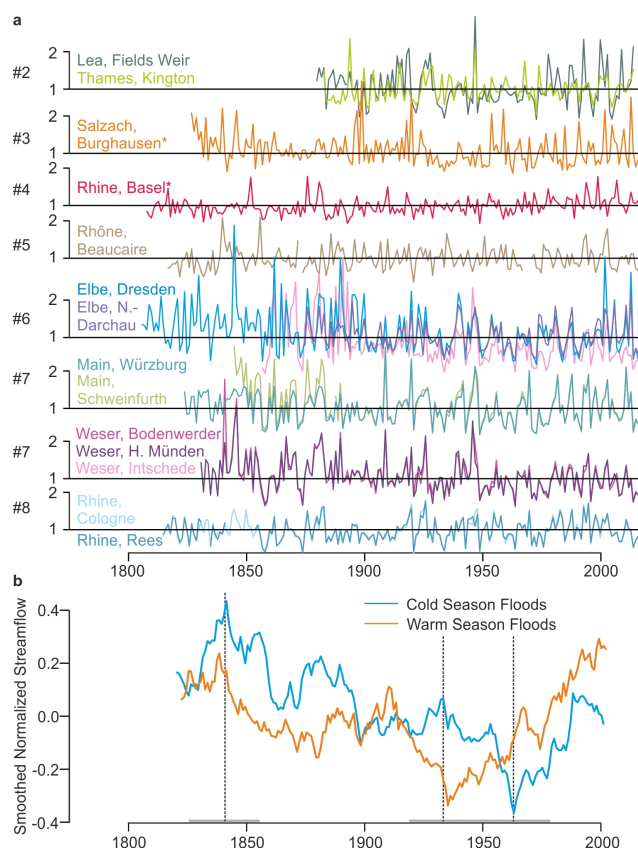
64 **2. Data and Methods**

65 *2.1. Annual peak streamflow series and daily precipitation series*

66 We use annual maximum streamflow from the Global Runoff Data Center (GRDC) from all series in
67 the region 42-60° N, 2° W to 18° E that are at least 110 years long (in 1904 / 1905 a network was
68 installed in Switzerland, hence coverage increases; one obviously inhomogeneous series from Sweden
69 was excluded). This set was supplemented with long daily streamflow series from the Rhône (Lang et



70 al., 2016) and Rhine (Wetter et al., 2011). This resulted in a set of 45 series (Table S1). For
71 comparison, all series were scaled with their 1901–2000 average. The fourteen longest series are
72 shown in Fig. 1a for illustration. For all further analyses, we normalized the series by fitting a Gamma
73 distribution (Botter et al., 2013) and transforming to the quantiles of a standard normal distribution
74 (we also analysed the raw data, which gave similar results). We term these series “flood intensity”,
75 noting that not each annual value would be called a “flood”.



76

77 **Figure 1. a** Scaled series of annual peak streamflow for the 14 longest series in Central Europe (Table S1,
78 numbers on the left refer to the regions defined in Sect. 2.2). Stars denote streamflow series with predominantly
79 summer floods. **b** Normalized series of annual peak streamflow averaged for rivers with predominantly cold-
80 season floods (blue) and warm-season floods (orange), smoothed with a 30-yr moving average (50% of rivers
81 must have data, first and last 15 years omitted). Dashed lines with grey bars show the 30-yr intervals chosen for
82 analysis.

83 To each of the streamflow series a daily precipitation record from a neighbouring station was assigned.
84 For this, we searched GHCN daily (Vose et al., 1992), ECAD (Klein Tank et al., 2002) as well as
85 series from MeteoSwiss, and selected series that are as long as possible and, if possible, from a
86 location upstream of the streamflow series (Table S1). Note that in some regions long precipitation
87 records are sparse, and in some cases the same precipitation record was used for more than one



88 streamflow record. Furthermore, it should be noted that these series have not been homogenized and
89 their long-term stability is questionable. From the precipitation series we calculated Rx5d and Rx20d,
90 *i.e.*, the annual maxima of precipitation sum over periods of 5 and 20 days, respectively.

91

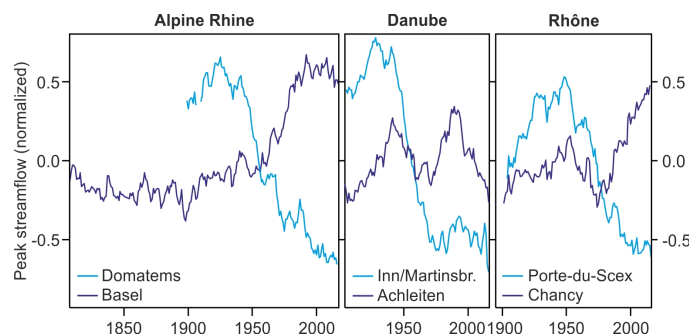
92 2.2. Regionalisation

93 In a next step, the streamflow series were grouped into regions with hydro-meteorological
94 characteristics as similar as possible using Ward clustering (Ward.D2 in R). We considered the
95 seasonalities of annual maximum streamflow, Rx5d, and Rx20d (*i.e.*, the probability of annual
96 maximum of precipitation over a 5-day window or peak stream flow to fall into a specific month, Fig.
97 S1), the coordinates of the river gauge as well as the coordinates of the precipitation station. The series
98 were standardized and scaled such that streamflow, precipitation, river coordinates, and precipitation
99 coordinates each contributed the same variance. A separation into nine clusters resulted in mostly
100 regionally coherent, non-overlapping clusters. One cluster comprised series from two different
101 catchments (Elbe, Danube) and was correspondingly split and merged with the existing Danube cluster
102 and with an Elbe sub-cluster. Additionally, one river (Ilz) was moved from the Danube cluster
103 (although the Ilz is a tributary of the Danube) to the central Germany cluster as the flood seasonality is
104 clearly distinct from that of the Danube (Fig. S2).

105 Within the Alpine clusters (Rhône, Alpine Rhine, Danube), individual peak streamflow series show
106 strikingly different trends (Fig. 2). Apart from the fact that the flood season changes from summer (in
107 the Alps) to winter (in the lowland) in all three rivers, which is partly reflected in the clustering as the
108 change occurs relatively far away from the Alps, also long-term trends radically change from the Alps
109 to the Alpine foreland. The highest catchments (mean elevation >2000 m asl) in all three regions
110 (Rhône, Porte-Du-Scex; Rhine Domatems; Inn Martinsbruck) show a strong decrease since the early
111 20th century, whereas the long-term evolution further downstream is flat (Rhône, Chancy) or
112 increasing (Rhine, Basel; Danube, Achleiten, Fig. 2). A possible explanation relates to the role of
113 snow processes on high-altitude catchments. Trends could then be due to a superposition of the
114 seasons of snow melt and heavy precipitation in the early 20th century, whereas the two seasons are
115 more separated today (FOEN, 2021). Other explanations include the role of power plants or other
116 hydraulic constructions on the flood regime. In any case, since the focus of this study is on
117 atmospheric processes, these rivers might confuse our results and hence we removed five series from
118 the three clusters. A one-series cluster in Sweden (Glomma) also is clearly affected by snow melt and
119 rain-on-snow events (Bøe et al., 2006). The series are shown in Fig. S3, but not further studied in
120 relation to atmospheric processes. Our final selection, shown in Fig. 3, comprises a set of 39
121 streamflow series, aggregated into eight clusters with areas of ca. 50,000-100,000 km². The clusters
122 are spatially coherent, internally consistent with respect to seasonality and heavy precipitation regime,
123 and internally homogeneous with respect to time evolution (exceptions are Southern England, where



124 the only two long series disagree, the Danube, where time evolution is less homogeneous, and perhaps
125 Central Germany where all series agree closely except for the Aller). The clusters represent Southern
126 England, Southern Norway, the Rhône, the Alpine Rhine, the Lower Rhine, Central Germany, the
127 Elbe, and the Danube.



128

129 **Fig. 2.** Normalized smoothed streamflow series for the three Alpine regions. In each region an upstream
130 catchment (mean altitude >2000 m asl, light blue) and streamflow series downstream from the same river system
131 (dark blue) is shown. All series are smoothed with a 30-yr moving average.

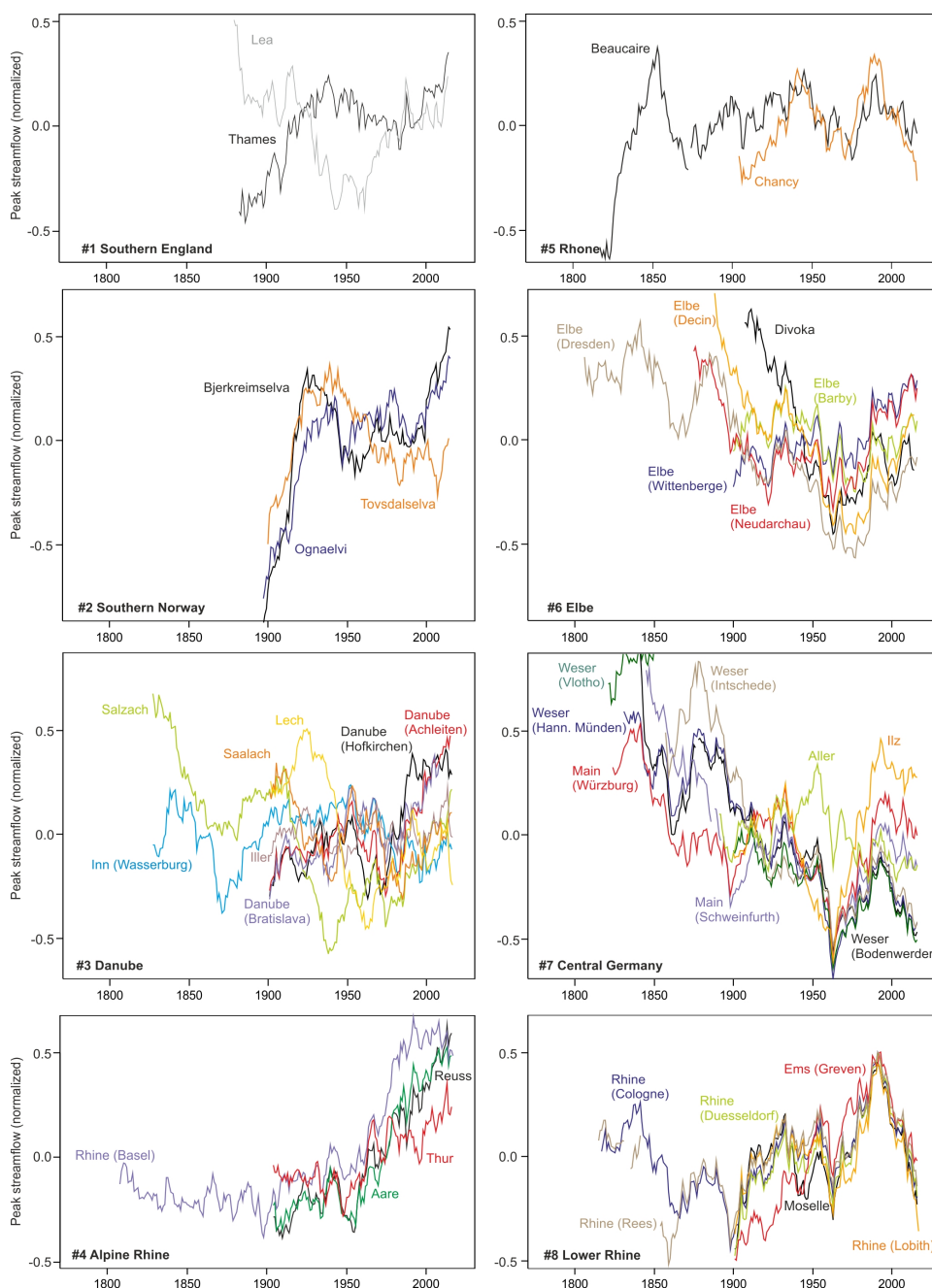
132

133 2.3. Atmospheric and climate data

134 The focus of the paper is on the atmospheric contribution to flood intensity. However, studying
135 atmospheric circulation 200 years back in time with a focus on extreme weather events is challenging.
136 To compensate for potential deficiencies of long-term data sets and to obtain more robust results, we
137 use multiple atmospheric data sets that are partly independent and are based on different methods.

138 The dynamical reanalysis 20CRv3 (Slivinski et al., 2019) provides 3-hourly, 3-dimensional, global
139 atmospheric data back to 1806. 20CRv3 assimilates only surface pressure observations into an
140 atmospheric model with prescribed sea-surface temperatures, sea-ice concentration, and radiative
141 forcings. It consists of 80 equally likely members. All analyses shown here were performed for each
142 member to obtain a physically plausible range of realisations. We extracted one grid point per region
143 (crosses in Fig. 4; selected from the $1 \times 1^\circ$ grid such as to best represent atmospheric processes relevant
144 for the region). The reanalysis allows calculating specific diagnostics, such as moisture flux
145 convergence, at a relatively high resolution. However, the quality of 20CRv3 varies in time and space,
146 particularly during the 19th century. The data prior to 1836 are less well evaluated and have a larger
147 uncertainty (Slivinski et al., 2021).

148 The second data set consists of daily weather types. Floods occur during specific weather patterns with
149 similar hydro-meteorological characteristics (Stucki et al., 2012) and thus weather type classifications
150 can be useful to study atmospheric contributions to floods. We use the Swiss CAP7 weather types
151 back to 1763 (Cluster Analysis of Principal Components, Schwander et al., 2017) which is based on
152 daily meteorological data from Europe, some of which overlap with 20CRv3.



153

154

155

Fig. 3. Normalized smoothed streamflow series for all series in all eight clusters. All series are smoothed with a 30-yr moving average.

156

157

158

The third data set is the updated global atmospheric paleo-reanalysis EKF400v2 covering the last 400 years (Franke et al., 2020; Valler et al., 2021). EKF400v2 provides monthly global 3-dimensional reconstructions from an offline assimilation. While there is a small overlap in input data with 20CRv3



159 (some of the pressure series), EKF400v2 mainly assimilates other data (temperature, precipitation,
160 documentary data, tree-rings). However, unlike for the other two data sets, we have no daily
161 resolution. We use the monthly values to analyse seasonal precipitation and 500 hPa geopotential
162 height (GPH).

163 For comparison with climate model data, we analyse monthly precipitation also directly in station data
164 (Peterson and Vose, 1997; Alexander and Jones, 2001; Murphy et al., 2018) and in the observation-
165 based gridded product HISTALP (Efthymiadis et al., 2006), which also includes temperature (note that
166 these data were assimilated into EKF400v2).

167

168 *2.4. Flood probability index*

169 Based on the weather types, we define a Flood Probability Index (FPI see below), which characterizes
170 a season or year based on sequences of weather types. To calibrate the index we need daily streamflow
171 series, which are available for only for the Rhine (Basel) and Rhône (Beaucaire). We calculate it
172 separately for the warm season (May to October, for Basel) and cold season (November to April,
173 Beaucaire) in order analyse the seasonally-varying relation of weather types with temperature
174 anomalies. The calculation of the FPI is based on Quinn and Wilby (2013) and is performed exactly as
175 in Brönnimann et al (2019). We first determined the 98th percentile of daily streamflow within the
176 respective seasonal window and marked all days above this percentile as extreme events. Events
177 separated by 3 or fewer days were combined to ensure independence, and from each sequence of
178 marked days only the day of the maximum was kept. For each weather type we then calculated the
179 fraction of days coinciding with a flood event relative to all days of that type. Then we assigned this
180 number to each day of that weather type. This was repeated for different lead times up to 5 days such
181 that the weather on preceding days is also considered. Lead times 5 to 0 were weighted as in
182 Brönnimann et al. (2019): 1/16, 1/8, 3/16, 1/4, 1/4, and 1/8. This yields an FPI for each day in the past
183 (note that the index was calibrated in the data after 1900, but calculated back to 1763). The 75th
184 percentile of this index calculated for each season was then chosen as an indicator of flood probability
185 (for details see Brönnimann et al., 2019).

186

187 *2.6. Water flux convergence*

188 Atmospheric circulation was furthermore analysed in terms of advection and convection of moist air.
189 We calculated a simplified measure of moisture flux convergence in which 850 hPa horizontal wind is
190 multiplied with precipitable water, termed water flux convergence in the following. This was
191 calculated for each of the 80 ensemble members of 20CRv3 and each 3-hour interval. In this analysis
192 we use the annual maximum 5-day average, CONV5d (analog to Rx5d; different windows from 3
193 hours to 10 days gave very similar results). All series were smoothed with a 30-year moving average



194 and finally the members were averaged. CONV5d indicates intense moisture transport and
 195 precipitation.

196 Based on the 3-hourly values feeding in to the maximum 5-day value, we decomposed CONV5d into
 197 its contributions as follows (overbar denotes the average over the entire period (1806-2015), primes
 198 denote deviations therefrom, q denotes precipitable water, \vec{v} is the wind vector):

$$\begin{aligned}
 & -\vec{v} \cdot \left((\bar{q} + q') \cdot (\vec{v} + \vec{v}') \right) = \\
 & -\bar{q} \cdot \left(\frac{\partial \bar{u}}{\partial x} + \frac{\partial \bar{v}}{\partial y} \right) - \bar{u} \cdot \frac{\partial \bar{q}}{\partial x} - \bar{v} \cdot \frac{\partial \bar{q}}{\partial y} \\
 & -\bar{q} \cdot \left(\frac{\partial u'}{\partial x} + \frac{\partial v'}{\partial y} \right) - u' \cdot \frac{\partial \bar{q}}{\partial x} - v' \cdot \frac{\partial \bar{q}}{\partial y} \\
 & -q' \cdot \left(\frac{\partial \bar{u}}{\partial x} + \frac{\partial \bar{v}}{\partial y} \right) - \bar{u} \cdot \frac{\partial q'}{\partial x} - \bar{v} \cdot \frac{\partial q'}{\partial y} \\
 & -q' \cdot \left(\frac{\partial u'}{\partial x} + \frac{\partial v'}{\partial y} \right) - u' \cdot \frac{\partial q'}{\partial x} - v' \cdot \frac{\partial q'}{\partial y}
 \end{aligned}$$

199
 200 This decomposition results in four groups of three terms. The first three terms on the right hand side
 201 (second line) indicate the contribution by the mean flow, the next three terms (third line) the
 202 contribution by changes in circulation (while keeping moisture constant), the next three terms measure
 203 the contribution by changes in precipitable water (while keeping the circulation constant) and the last
 204 three terms describe the interaction of circulation and moisture changes.

205

206 2.7. Model simulations

207 To test the effect of sea-surface temperature and external forcing on multidecadal variations of
 208 atmospheric circulation, we used the global atmospheric model ECHAM6 (Giorgetta et al., 2013). It
 209 was run in the standard configuration T63L47 for the years 1851-2015. The spatial resolution
 210 corresponds to ca. 1.9°. In total 31 members were produced using different initial conditions as well as
 211 different sea-surface temperatures (obtained by sampling from the ten members in HadISST2); only
 212 one realization was available for sea ice (Titchner and Rayner, 2014). All other forcings (land surface,
 213 volcanic aerosols, tropospheric aerosols, and greenhouse gas concentrations) followed the PMIP
 214 protocol (Jungclaus et al., 2017). Ensembles with individual forcings are not available.

215

216 3. Results and Discussion

217 3.1. Annual peak streamflow

218 The longest 14 series show that extreme floods occurred in the 19th century, particularly in the Elbe,
 219 Weser, and Main catchments, but also Salzach and Rhône show high peaks. Conversely, apart from
 220 floods in 1946 (Weser) and 1947 (Lea, Thames, Main), the period ca. 1940 to 1970 exhibits fewer
 221 spikes. However, the rivers exhibit different streamflow regimes and flood seasonalities (Fig. S2). The



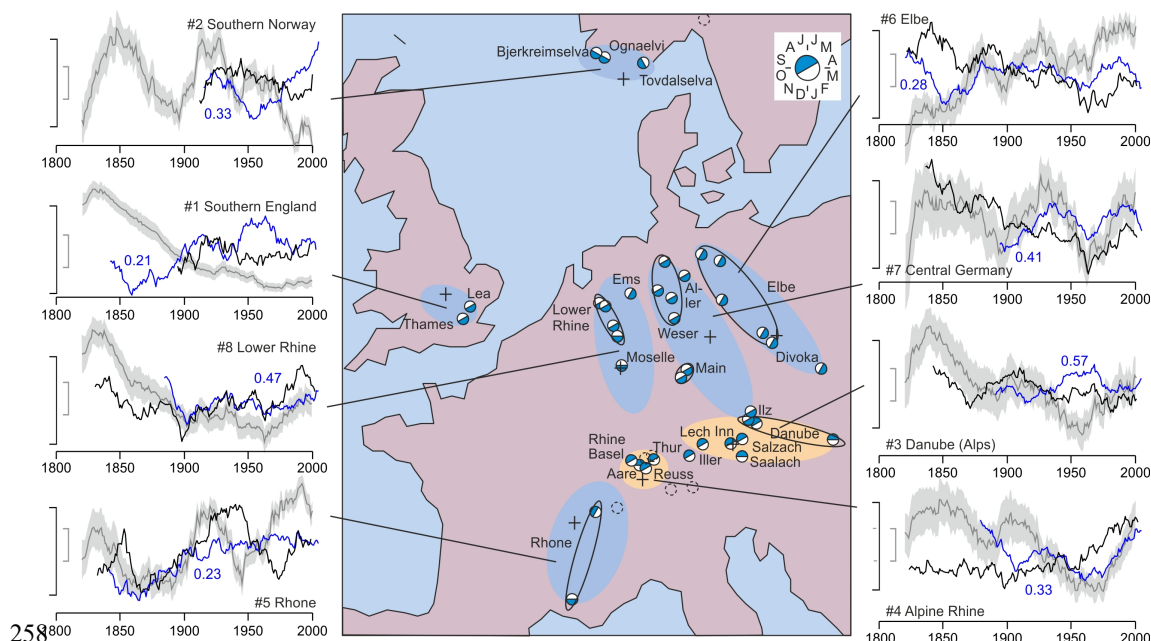
222 upper (Alpine) catchments of Rhine and Danube exhibit their annual maximum streamflow typically
223 during the warm season, most other catchments during the cold season. After normalizing, the “cold
224 season” and “warm season” rivers were therefore averaged separately and the series were smoothed in
225 Fig. 1b. Likewise, all further analyses were performed for annual series as well as for flood seasons
226 (i.e., Nov-Apr for “cold season” flood rivers and May-Oct for “warm season” flood rivers).

227 These aggregated curves show additional features, such as a less pronounced peaks for cold-season
228 flood rivers are found in the 1870s and the early 20th century. Based on peaks on the cold-season
229 series, three 30-yr periods were selected for further investigation: 1827-1856 (primary maximum),
230 1949-1978 (primary minimum), and 1919-1948 (local maximum; interesting as the warm-season
231 series exhibit low values). While numerous non-climatic factors (e.g., changes in the stream network
232 and land use) contribute to long term trends, multidecadal variability is less influenced by such
233 changes and hence climatic conditions are analysed.

234 Our findings of increased flood intensities in Central Europe in the 19th century and a decrease in the
235 mid-20th century are confirmed by documentary evidence (Naulet et al., 2005; Wetter et al., 2011;
236 Himmelsbach et al., 2015; Lang et al., 2016). A recent, comprehensive study based on documentary
237 data and a three-class flood magnitude index (Blöschl et al., 2020) found coherent flood phases in the
238 mid-19th century in Central and Southern Europe, in the early 20th century in northwestern Europe, and
239 in recent decades in Central and Western Europe, although this is not the case for each individual river
240 (Glaser et al., 2010).

241 Our aggregation into eight regions retains the main phases of flood intensity but adds spatial
242 information. This is shown for annual time series (Fig. S4) as well as for flood seasons (Fig. 4). High
243 peak streamflow occurred in Central Europe in the 19th century, in Central and Western Europe in the
244 early 20th century, low peak streamflow in all regions after 1950. Since 1970 peak streamflow has
245 increased, although not everywhere, and some series (not only those influenced by snow) show a
246 decline at the beginning of the 21st century.

247 For comparison with Blöschl et al. (2020), we add the interpolated and smoothed series calculated
248 from their data and code to Fig. S4. Correlations (at 4-yr aggregation) with peak streamflow (numbers
249 in Fig. 4) are between 0.4 and 0.52 except for Southern England. Obviously, the comparability of
250 measurement-based versus document-based evidence is limited. For instance, analysed statistics differ
251 (annual maxima versus indexed extremes), the series measure different aspects of flood (streamflow
252 versus documented flood intensity) and there is large river-to-river variability. Yet, the flood-rich
253 decades in the middle and late 19th century in Central Europe, in the early 20th century in Northwestern
254 Europe, the Europe-wide flood-poor period after 1950, and the recent increase in flood intensity are
255 salient features of all analyses. Hence, the regional characteristics are consistent with the documentary
256 evidence on a climatological scale, and the fact that corresponding periods of more and less frequent
257 floods are found with both methods opens the door for the following analyses.

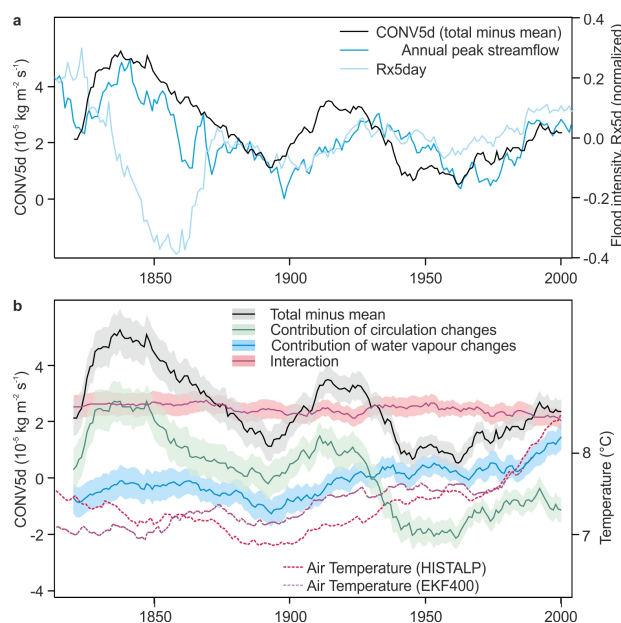


259 **Figure 4.** Regionally averaged (coloured ellipses; black ellipses indicate same river) series of normalized peak
 260 streamflow (black), Rx5day (blue, the number indicates its correlations with peak streamflow at 4-yr aggregation)
 261 and CONV5d during the flood season from 20CRv3 at locations of crosses (grey, shading indicates the ensemble
 262 standard deviation), standardized and subsequently smoothed with a 30-yr moving average (scale bars range
 263 from -0.5 to +0.5). Regions are colour-coded according to the predominance of cold (blue; Nov-Apr) or warm
 264 season floods (orange; May-Oct). The blue part of the white-blue circle for each river indicates the 6-month period
 265 with highest flood frequency). Dashed circles: Streamflow series excluded because of likely influence of snow
 266 melt, or hydropower dams or other hydraulic constructions on trends.

267 *3.2. Atmospheric influences and the role of circulation and water vapour changes*

268 First, we analysed the relation with precipitation. In most regions, flood intensities are statistically
 269 related to Rx5day. Correlations (Fig. 4, again calculated for 4-yr averages for consistency) are 0.21 to
 270 0.57. Hence, years with high peak stream flow coincide with years with high maximum 5-day
 271 precipitation. Note that neither peak stream flow nor Rx5day are based on homogenised data series.

272 Next, we analysed atmospheric influences on the multidecadal variability of peak stream flow using
 273 the diagnostics defined in Sect. 2. The CONV5d series (grey lines and shading in Fig. 4; for
 274 visualization they were standardized prior to filtering) exhibit multidecadal variations with maximum
 275 convergence in the 19th and early 20th century and minimum convergence around 1950, although the
 276 pattern differs from region to region. They are in general agreement with the maximum streamflow
 277 curves for several regions (e.g., Rhône, Lower Rhine, Central Germany, Danube), while in other
 278 regions the agreement is worse. Similarly as for Rx5day, CONV5d is less reliable in the early years,
 279 prior to ca. 1836. The steep increase in these years therefore cannot be assessed.



280

281 **Figure 5. a** Average of regional averages of annual maxima of peak streamflow, Rx5day, and CONV5d. **b**
282 Contributions to CONV5d from circulation changes, water vapour changes, and their interaction. Shading
283 indicates ± 1 std. dev. Dashed curves show annual mean temperature from HISTALP and EKF400. All curves are
284 smoothed with a 30-yr moving average.

285 While all individual indicators (flood intensity, Rx5day, CONV5d) have uncertainties that are
286 particularly large in the early decades, there are also clear similarities. A further aggregation reveals
287 the common low-frequency variability even more distinctly. When averaging all three indicators
288 across all eight regions (Fig. 5), we find a close similarity after around 1870. All series show the
289 recent increase, the minimum in the 1960s, a peak around the 1930s, and a minimum around 1900, as
290 already noted in Fig. 1. Flood intensity and CONV5d also show a peak in the 1840s, which is however
291 not seen in the (sparse) Rx5day data.

292 Thus, despite the uncertainties, we can use these indicators to trace the atmospheric impacts on the
293 multidecadal variability in flood intensity. The atmospheric processes, in turn, can be partitioned into
294 contributing processes as described in Sect. 2. Figure 5b shows the contributions from circulation
295 changes, from water vapour changes, and from their interaction. The interaction term is negative with
296 only small changes over time. The contribution from circulation changes (green line) dominates and
297 shows all main features found in CONV5d. However, the long term trend differs. This is due to
298 changes in water vapour (blue line). The contribution of water vapour changes shows a two-step
299 increase after 1900.

300 The contribution of water vapour changes depends on temperature through the Clausius-Clapeyron
301 relation. To illustrate this relation, annual mean temperature in HISTALP (Efthymiadis et al 2006), the
302 longest gridded observational data set, and in EKF400v2 for the same regions are plotted such that 1



303 °C corresponds to $0.46 \cdot 10^{-5} \text{ kg m}^{-2} \text{ s}^{-1}$. This is equivalent to a 6.5% change in CONV5d, the number
304 expected following the Clausius-Clapeyron relation if annual maxima would follow the annual
305 average trend (saturation can be assumed for annual maximum moisture convergence). After around
306 1900, the general pattern and amplitude of the contribution of water vapour changes is consistent with
307 an increased intensity of heavy precipitation in a warming atmosphere, although the amplitude of the
308 CONV5d increase is somewhat smaller than that of the scaled temperature increase.

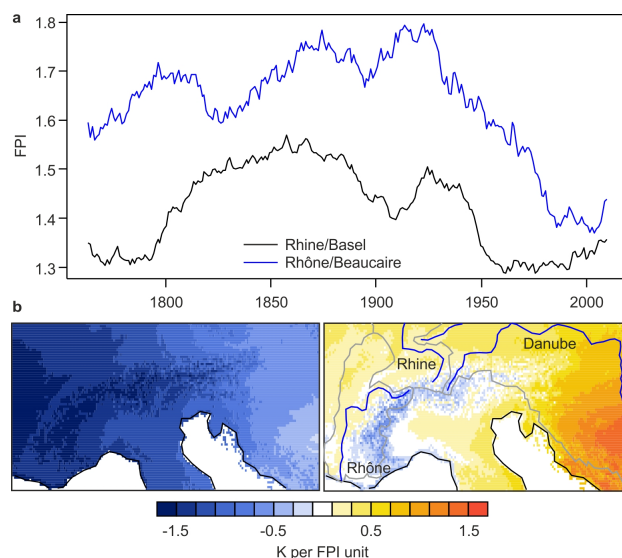
309 In fact, this might explain the varying relation between temperature and floods over time:
310 Palaeoclimate studies (Stewart et al 2011, Glur et al 2013), particularly from the northern Alps,
311 suggest that past flood-rich periods coincided with cool periods, while climate projections suggest that
312 with global warming, flood occurrence may increase in certain regions. To analyse the role of
313 circulation, we used the FPI index for the Rhône and Rhine, which was calculated specifically for the
314 corresponding flood seasons (Nov-Apr for the Rhône, May-Oct for the Rhine). This index measures
315 the frequency of flood-prone weather types, to which cyclonic weather types contribute very strongly.
316 As a consistency test, the smoothed curves (Fig. 6a) show high values in the 19th and early 20th century
317 and a decrease after ca. 1950; further analyses of the FPI index for Basel are shown in Brönnimann et
318 al. (2019). For the following analysis we used the unsmoothed, but detrended FPI indices, onto which
319 we regressed the detrended temperature fields of the corresponding seasons (Fig. 6b). For the Rhine,
320 which is mostly affected by summer floods, flood prone seasons are typically cold. Conversely, for the
321 Rhône, with typically winter floods, flood-prone seasons are warmer than average in the lowland, but
322 colder than average at higher altitudes. Both is consistent with a predominance of cyclonic weather
323 types: They bring colder than average weather in summer, but warmer than average in winter except at
324 high altitudes, which normally, but not during cyclonic weather types, are often above an inversion.

325 This means that from the contribution of circulation alone, flood-rich periods in summer-flood regions
326 and generally in the Alps are expected to be cool. This is not the case after 1980, when the partitioning
327 (Fig. 5b) shows a growing contribution of water vapour increase whereas the contribution of
328 circulation changes is constant (and the FPI is low, Fig. 6a).

329

330 *3.4. Regional differences in circulation effects*

331 Circulation changes had regionally different imprints in different times. Recall that 1827-1856 was
332 flood-rich in Central Europe (year-round), 1919-1948 was flood-rich in northern and western Europe
333 (cold season), 1949-1978 was flood-poor across Europe (year-round, Fig. 1). The contribution of
334 circulation changes to CONV5d (shown in Fig. 7 for each region) is consistent with this result. Some
335 regions show an almost opposite behaviour to each other. For instance, in the mid 19th century,
336 circulation changes contributed to high CONV5d in Southern Norway but to relatively low values in
337 the Rhône catchment, whereas the opposite was the case in the second half of the 20th century (Fig. 7).
338 While the contribution of circulation differs from region to region, the contribution from water
339 vapour changes is more uniform and shows an increase in all regions.



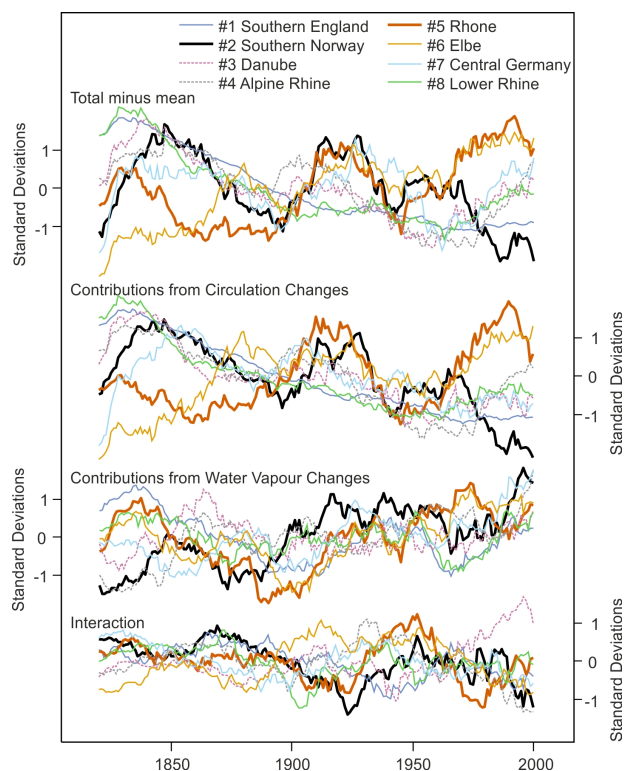
340

341 **Figure 6.** a. FPI index for the Rhine in Basel (May-Oct) and the Rhône in Beaucaire (Nov-Apr), smoothed with a
342 30-yr moving average. b. Regression map of detrended seasonal (May-Oct and Feb-Apr, respectively) mean
343 temperature in HISTALP onto the corresponding (detrended) FPI indices.

344 To test whether these spatial differences due to atmospheric circulation are reflected in the seasonal
345 mean large-scale flow, we analysed (Fig. 8) 30-yr averages of seasonal mean anomalies in
346 precipitation and 500 hPa GPH in EKF400v2 and observations (Peterson and Vose, 1997; Alexander
347 et al., 2001; Murphy et al., 2018). In terms of seasonal mean precipitation, the cold seasons 1827-1856
348 and 1949-1978 show a rather mixed signal. Although not inconsistent with the observed multidecadal
349 flood intensity, one would probably not address these periods as flood-rich and flood-poor,
350 respectively, based only on seasonal mean precipitation (note that Blöschl et al. (2020) define a flood
351 period in 1840-1872; corresponding plots exhibit similar patterns as for 1827-1856; Fig. S5).

352 The period 1827-1856 (cold season) shows a pressure pattern that is similar to a negative mode of the
353 North Atlantic Oscillation, but with the positive pressure anomaly displaced southeast of Iceland.
354 Seasonal mean precipitation (both in EKF400v2 and station data) shows a mixed signal; with slight
355 increases in the Rhône catchment, Central Europe, and Southern Norway, but drying over England. The
356 warm season shows negative anomalies of 500 hPa GPH over the entire continent, accompanied by
357 increased rainfall, which is consistent with frequent flood-prone weather.

358 The 1919-1948 cold season average shows negative 500 hPa GPH anomalies over the Atlantic and
359 increased precipitation over Western Europe, which agrees with the increased flood intensity in this
360 region. The clearest signal is found for the flood-poor period 1949-1978 in the warm season. The
361 analysis shows pronounced drying and positive anomalies of 500 hPa GPH. The start of this period,
362 which coincided with massive droughts (e.g., Brazdil et al., 2016) was accompanied by a poleward
363 shifted subtropical jet (Brönnimann et al., 2015).

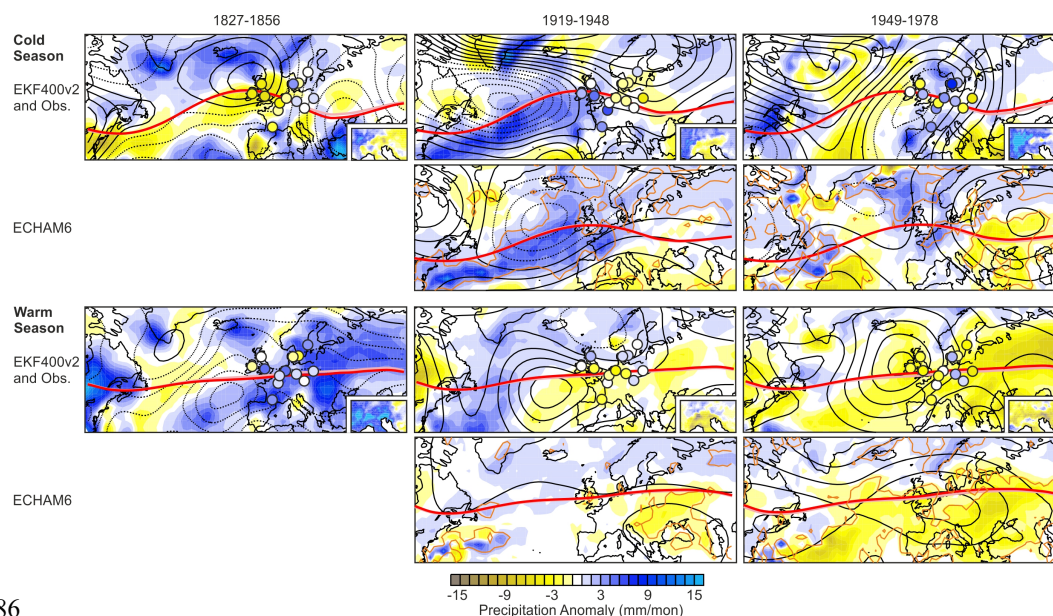


364
365 **Figure 7.** CONV5d (total minus mean) and contributions to it from circulation changes, water vapour changes,
366 and their interaction for each of the eight regions. All series were standardized and smoothed with a 30-yr moving
367 average.

368 We further addressed the underlying causes of multidecadal anomalies by analysing, in the same way
369 as EKF400v2, an ensemble of 31 simulations with the ECHAM6 atmospheric model starting in 1851
370 (the 1827-1856 period cannot be analysed). The precipitation anomalies and the broad features of
371 GPH anomalies found in EKF400v2 are rather well reproduced for the 1919-1948 and 1949-1978
372 periods, both cold and warm seasons (for 1840-1872 see Fig. S5). For instance, for the cold season, the
373 negative GPH anomalies over the North Atlantic in 1918-1948 and the zonal pattern of low GPH over
374 the eastern North Atlantic and high GPH over Russia in 1949-1978 agree well. The wet conditions in
375 western Europe in 1919-1948 in winter and the dry conditions in 1949-1978 in summer are highly
376 significant in the atmospheric model simulations. The latter is arguably the most significant feature in
377 the model analysis. Although this analysis concerns only changes in the seasonal means, not in
378 extremes, it shows that atmospheric model simulations forced with, among other factors, sea-surface
379 temperatures are able to reproduce some characteristic features of atmospheric circulation changes.
380 However, the seasonal mean circulation and precipitation describes the flood conditions only to a
381 limited extent (see Zanchettin et al., 2019, for the role of Atlantic sea-surface temperature variability
382 for floods). Note, also, that also EKF400v2, despite the large number of observations assimilated, is



383 dependent on sea-surface temperature input to the underlying model. Overall, the model simulations
384 suggest that part of the multidecadal variability can be reproduced from model boundary conditions
385 (sea-surface temperature, external forcings).



386
387 **Figure 8.** Simulated atmospheric circulation and precipitation. Anomalies (with respect to 1851-1950) of
388 precipitation (colours) and 500 hPa GPH (contour distance 2 gpm centered around zero, dashed contours
389 indicate negative numbers) in the 30-yr periods 1827-1856, 1919-1948, and 1949-1978 in the EKF400v2
390 reconstruction (ensemble mean), observations (insets: HISTALP; circles: GHCN), and ECHAM6 simulations
391 (hatching denotes 95% significance of precipitation anomalies, calculated from the 30-year averages of the 31
392 members using a one-sample t-test). Thick red lines show the GPH contour 5450 gpm (cold season) or 5650 gpm
393 (warm season; light pink: same for 1851-1950).

394

395 5. Conclusions

396 Long time series of annual peak streamflow in Western and Central Europe exhibit substantial
397 multidecadal variability, consistent with previous work by other authors. Flood-rich phases occurred in
398 the 19th century in several regions, in the early 20th century in western and northern Europe, and since
399 the 1980s, while a flood-poor period occurred after the second world war. The flood variability is in
400 line with observed changes in Rx5day (except in the mid-19th century, which however could be due to
401 a lower data quality).

402 Annual peak atmospheric water flux convergence in a reanalysis also shows the same pattern of
403 multidecadal variability as flood intensity and Rx5day, and this is further supported by an indicator
404 based on weather types. Although the uncertainties in each data set are large, results are robust and



405 show the same main phases of low-frequency variability. The reanalysis data allow a more physical
406 interpretation. Partitioning the atmospheric water flux convergence into contributions from circulation
407 and water vapour changes, we find that peak streamflow of European rivers from around 1820 to 1980
408 was largely forced by atmospheric circulation changes. In contrast, the recent increase in moisture flux
409 convergence was to a larger part driven by increasing atmospheric moisture due to climate change.
410 This explains why in the past, flood-rich periods coincided with cold periods (particularly in summer-
411 flood regions such as the northern Alps, to which many proxy studies refer) while more floods may be
412 possible in Europe in a future, warming climate.

413 Changes in seasonal mean atmospheric circulation partly mirror the changes in flood intensity
414 changes. Important features of these changes are reproduced in atmospheric model simulations,
415 indicating that oceanic forcing might play a role. This is specifically the case for the dry and flood-
416 poor summers 1949-1978.

417 The thermodynamic effect is likely to increase further. The floodings in Central and Western Europe
418 the summer of 2021 fit into the picture of a stronger thermodynamic contribution. However, flood
419 projections in Europe under different emission scenarios remain unclear (Kundzewicz et al., 2017), as
420 several sources of uncertainties have to be considered (climate models, downscaling, hydrological
421 models) and projections for flood intensity (e.g. Roudier et al., 2016), frequency (e.g. Giuntoli et al.,
422 2015) or both (e.g. Alfieri et al., 2015) in European rivers vary.

423

424 *Acknowledgements:* This work was supported by Swiss National Science Foundation project WeaR (188701),
425 and by the European Commission (ERC Grant PALAEO-RA, 787574). Simulations were performed at the Swiss
426 National Supercomputing Centre CSCS. Support for the Twentieth Century Reanalysis Project version 3 dataset
427 is provided by the U.S. Department of Energy, Office of Science Biological and Environmental Research (BER),
428 by the National Oceanic and Atmospheric Administration Climate Program Office, and by the NOAA Physical
429 Sciences Laboratory. We acknowledge the data providers in the ECA&D project.

430 References

- 431 Alexander, L. V. and Jones, P. D.: Updated precipitation series for the UK and discussion of recent extremes, *Atmos. Sci.*
432 *Lett.* doi:10.1006/asle20010025, 2001.
- 433 Alfieri, L., Burek, P., Feyen, L. and Forzieri, G.: Global warming increases the frequency of river floods in Europe, *Hydrol.*
434 *Earth Syst. Sci.*, 19, 2247–2260, 2015.
- 435 Alfieri, L., Bisselink, B., Dottori, F., Naumann, G., de Roo, A., Salamon, P., Wyser, K. and Feyen, L.: Global projections of
436 river flood risk in a warmer world. *Earth's Future*, 5, 171-182, 2017.
- 437 Blöschl, G. et al.: Current flood-rich period exceptional compared to past 500 years in Europe *Nature*, 583, 522-524, 2020.
- 438 Bøe, A.-G., Dahl, S. O., Lie, Ø. and Nesje, A.: Holocene river floods in the upper Glomma catchment, southern Norway: a
439 high-resolution multiproxy record from lacustrine sediments, *The Holocene*, 16, 445-455, 2006.
- 440 Botter, G., Basso, S., Rodriguez-Iturbe, I. and Rinaldo, A.: Resilience of river flow regimes, *Proc. Natl. Acad. Sci.*, 110,
441 12925-12930, 2013.
- 442 Brázdil, R., Pfister, C., Wanner, H., von Storch, H. and Luterbacher, J.: Historical climatology in Europe – the state of the art,
443 *Clim. Change.*, 70, 363–430, 2005.



- 444 Brázdil, R. et al.: The Central European drought of 1947: causes and consequences, with particular reference to the Czech
445 Lands, *Clim. Res.*, 70, 161-178, 2016.
- 446 Brönnimann, S. et al.: Southward shift of the Northern tropical belt from 1945 to 1980, *Nat. Geosci.*, 8, 969-974, 2015.
- 447 Brönnimann, S. et al.: Causes for increased flood frequency in central Europe in the 19th century, *Clim. Past.*, 15, 1395–
448 1409, 2019.
- 449 Efthymiadis, D. et al.: Construction of a 10-min-gridded precipitation data set for the Greater Alpine Region for 1800–2003,
450 *J. Geophys. Res.*, 111, D01105, 2006.
- 451 Engeland, K. et al.: New flood frequency estimates from the largest river in Norway based on the combination of short and
452 long time series, *Hydrol. Earth Syst. Sci.*, 24, 5595-5619, 2020.
- 453 Franke, J., Valler, V., Brugnara, Y. and Brönnimann, S.: Ensemble Kalman Fitting Paleo-Reanalysis Version 2 (EKF400_v2)
454 World Data Center for Climate (WDCC) at DKRZ https://doi.org/10.26050/WDCC/EKF400_v20, 2020.
- 455 Giorgetta, M. A. et al.: *The atmospheric general circulation model ECHAM6 - Model description*, Reports on Earth System
456 Science, 135, 2013.
- 457 Giuntoli, I., Vidal, J.-P., Prudhomme, C. and Hannah, D. M.: Future hydrological extremes: The uncertainty from multiple
458 global climate and global hydrological models, *Earth Syst. Dyn.*, 6, 267–285, 2015.
- 459 Glaser, R. et al.: Floods in Central Europe since AD 1300 and their regional context, *La Houille Blanche*, 5, 43-49, 2004.
- 460 Glaser, R. et al.: The variability of European floods since AD 1500, *Clim. Change.*, 101, 235–256, 2010.
- 461 Glur, L. et al.: Frequent floods in the European Alps coincide with cooler periods of the past 2500 years, *Sci. Rep.*, 3, 2770,
462 2013.
- 463 Hall, J. et al.: Understanding flood regime changes in Europe: a state-of-the-art assessment, *Hydrol. Earth Syst. Sci.*, 18,
464 2735–2772, 2014.
- 465 Himmelsbach, I., Glaser, R., Schoenbein, J., Riemann, D. and Martin, B.: Reconstruction of flood events based on
466 documentary data and transnational flood risk analysis of the Upper Rhine and its French and German tributaries since
467 AD 1480, *Hydrol. Earth Syst. Sci.*, 19, 4149–4164, 2015.
- 468 Jacobeit, J., Glaser, R., Luterbacher, J., and Wanner, H.: Links between flood events in Central Europe since AD 1500 and
469 largescale atmospheric circulation modes, *Geophys. Res. Lett.*, 30, 1172–1175, 2003.
- 470 Jungclaus, J. H. et al.: The PMIP4 contribution to CMIP6 – Part 3: The last millennium scientific objective and experimental
471 design for the PMIP4 past1000 simulations, *Geosci. Model Dev.*, 10, 4005-4033, 2017.
- 472 Klein Tank, A.M.G. et al.: Daily dataset of 20th-century surface air temperature and precipitation series for the European
473 Climate Assessment, *Int. J. Climatol.*, 22, 1441-1453, 2002.
- 474 Kundzewicz, V. et al.: Differences in flood hazard projections in Europe – their causes and consequences for decision
475 making, *Hydrol. Sci. J.*, 62, 1-14, 2017.
- 476 Lang, M., Coeur, D., Audouard, A., Villanova-Oliver, M. and Pène, J.-P.: BDHI: a French national database on historical
477 floods E3S Web Conf 7 04010, 2016.
- 478 Mudelsee, M., Börngen, M., Tetzlaff, G. and Grünewald, U.: Extreme floods in central Europe over the past 500 years: Role
479 of cyclone pathway “Zugstrasse Vb”, *J. Geophys. Res.*, 109, D23101, 2004
- 480 Murphy, C. et al.: A 305-year continuous monthly rainfall series for the island of Ireland (1711–2016), *Clim. Past*, 14, 413–
481 440, 2018.
- 482 Naulet, R. et al.: Flood frequency analysis on the Ardèche river using French documentary sources from the last two
483 centuries, *J. Hydrol.*, 313, 58–78, 2005.
- 484 Peterson, T. C. and Vose, R. S.: An overview of the Global Historical Climatology Network temperature database, *B. Amer.*
485 *Meteorol. Soc.*, 78, 2837-2849, 1997.
- 486 Pfister, C.: Die „Katastrophenlücke“ des 20 Jahrhunderts und der Verlust traditionellen Risikobewusstseins, *Gaia*, 18, 239–
487 246, 2009.
- 488 Quinn, N. and Wilby, R. L.: Reconstructing multi-decadal variations in fluvial flood risk using atmospheric circulation
489 patterns, *J. Hydrol.*, 487, 109-121, 2013.
- 490 Roudier, P. et al.: Projections of future floods and hydrological droughts in Europe under a +2°C global warming, *Clim.*
491 *Change*, 135, 341–355, 2016.



- 492 Schmocker-Fackel, P. and Naef, F.: Changes in flood frequencies in Switzerland since 1500 Hydr Earth Sys Sci 14 1581–
493 1594, 2010a
- 494 Schmocker-Fackel, P. and Naef, F.: More frequent flooding? Changes in flood frequency in Switzerland since 1850, J.
495 Hydrol., 381, 1–8, 2010b.
- 496 Schwander, M. et al.: Reconstruction of Central European daily weather types back to 1763, Int. J. Climatol., 37, 30–44,
497 2017.
- 498 Slivinski, L. C. et al.: An evaluation of the performance of the 20th Century 1 Reanalysis version 3, J. Clim., 34, 1417–1438,
499 2021.
- 500 Slivinski, L. C. et al.: Towards a more reliable historical reanalysis: Improvements to the Twentieth Century Reanalysis
501 system, Q. J. Roy. Meteorol. Soc., 145, 2876–2908, 2019.
- 502 Stewart, M. M., Grosjean, M., Kuglitsch, F. G., Nussbaumer, S. U. and von Gunten, L.: Reconstructions of late Holocene
503 paleofloods and glacier length changes in the Upper Engadine Switzerland (ca 1450 BC–AD 420), Palaeogeogr.
504 Palaeocl., 311, 215–223, 2011.
- 505 Stucki, P. et al.: Five weather patterns and specific precursors characterize extreme floods in Switzerland, Meteorol. Z., 21,
506 531–550, 2012.
- 507 Summermatter, S.: *Die Überschwemmungen von 1868 in der Schweiz Unmittelbare Reaktion und längerfristige Prävention*
508 *mit näherer Betrachtung des Kantons Wallis*, Nordhausen, T. Bautz, 2005
- 509 Tarasova, L. et al.: Causative classification of river flood events, WIREs Water, 6, e1353, 2019.
- 510 Titchner, H. A. and Rayner, N. A.: The Met Office Hadley Centre sea ice and sea surface temperature data set version 2: 1
511 Sea ice concentrations, J. Geophys. Res., 119, 2864–2889, 2014.
- 512 Valler, V., Franke, J., Brugnara, Y. and Brönnimann, S.: An updated global atmospheric paleo-reanalysis covering the last
513 400 years, Geosc. Data J., doi: 101002/gdj3121, 2021.
- 514 Vose, et al.: *The Global Historical Climatology Network: Long-term monthly temperature, precipitation, sea level pressure,*
515 *and station pressure data*, Oak Ridge National Laboratory Environmental Sciences Division Publ. 3912, 324 pp, 1992.
- 516 Wetter, O. et al.: The largest floods in the High Rhine basin since 1268 assessed from documentary and instrumental
517 evidence, Hydrol. Sci. J., 56, 733–758, 2011.
- 518 Zanchettin, D. et al.: Atlantic origin of asynchronous European interdecadal hydroclimate variability, Sci. Rep., 9, 10998,
519 2019.

520 **Data availability**

521 The GRDC data can be downloaded here: https://www.bafg.de/GRDC/EN/Home/homepage_node.html

522 Flood series on the Rhône river at Beaucaire (1816–2016) is available from: [https://www.plan-](https://www.plan-rhone.fr/publications-131/actualisation-de-lhydrologie-des-crues-du-Rhone-1865.html?cHash=5628938abe287dc9ca390dad7373ae0e)

523 [Rhône.fr/publications-131/actualisation-de-lhydrologie-des-crues-du-Rhône-](https://www.plan-rhone.fr/publications-131/actualisation-de-lhydrologie-des-crues-du-Rhone-1865.html?cHash=5628938abe287dc9ca390dad7373ae0e)

524 [1865.html?cHash=5628938abe287dc9ca390dad7373ae0e](https://www.plan-rhone.fr/publications-131/actualisation-de-lhydrologie-des-crues-du-Rhone-1865.html?cHash=5628938abe287dc9ca390dad7373ae0e)

525 EKF400v2.0 is available from: https://doi.org/10.26050/WDC/EKF400_v2.0, 2020

526 20CRv3 is available here: https://portalnersc.gov/project/20C_Reanalysis/

527 HISTALP is available here: <http://www.zamg.ac.at/histalp/datasets.php>

528 The CAP7 weather types are available from <https://cp.copernicus.org/articles/15/1395/2019/>, the Lamb weather

529 types are available from <https://doi.pangaea.de/10.1594/PANGAEA.896307>

530 **Code availability**

531 The code for the processing of the streamflow data as well as for generating the FPI is attached as supplementary
532 file together with all input data.

533 **Author contributions**

534 SB designed the studies and did most of the analyses and writing. PS processed reanalysis data, JF, VV, and YB

535 provided the EKF400v2 data and helped in the analysis, RH performed the climate model simulations, LCS,

536 GPC and PDS provided the 20CRv3 reanalysis data and interpretation, ML provided the Rhône data and BS

537 assisted in the hydrological analyses. ML and BS assisted in the hydrological interpretations. All authors actively

538 discussed the results and all authors contributed to writing.